AIAA JOURNAL
Vol. 45, No. 11, November 2007

Dynamic Fracture Analysis of Adhesively Bonded Joints Using Explicit Methods

Dhaval P. Makhecha,* Rakesh K. Kapania,† Eric R. Johnson,‡ and David A. Dillard§
Virginia Polytechnic Institute and State University, Blacksburg, Virginia 24060

DOI: 10.2514/1.26088

Dynamic fracture tests of adhesively bonded double-cantilever beams subjected to impact loading from a falling wedge in a drop-tower fixture are presented. Dynamic simulations of the fracture tests are performed using the explicit method available in the commercial software LS-DYNA. A cohesive zone model for fracture of the adhesive is implemented as a user-defined material in LS-DYNA. Simulations of the double-cantilever beams with aluminum adherends correlated very well with the test data. To achieve good correlation with the test for the double-cantilever beams with composite adherends, the measured displacement history of the tip of the adherend in contact with the falling wedge had to be implemented as a boundary condition in the simulation.

Nomenclature

a	=	crack length
B	=	width of the beam
d	=	damage parameter
E_f	=	modulus of elasticity of the adherend material
F	=	correction factor for large deflection
G_{I}	=	strain energy release rate for mode I
G_{I_c}	=	critical strain energy release rate in mode I
G_{II_c}	=	critical strain energy release rate in mode II
G_{III_c}	=	critical strain energy release rate in mode III
h	=	thickness of the adhesive
I	=	moment of inertia of the beam
T_1^c, T_2^c, T_3^c	=	relative maximum tractions in the adhesive in modes II, III, and I
t	=	time
x	=	position along the beam
β	=	brittleness parameter
$\Gamma[z]$	=	Euler gamma function of argument z
$\bar{\Delta}_i$	=	Δ_i/Δ_i^c
Δ_1, Δ_2, Δ_3	=	displacements across the crack faces in modes II, III, and I
δ	=	opening displacement at a given x
δt	=	time increment
κ	=	interpenetration factor
μ	=	mixed-mode parameter
ρ	=	density of the material
ϕ	=	shear angle in the adhesive

I. Introduction

ADHESIVELY bonded joints are widely regarded as an alternative to traditional bonding methods such as riveting and welding because they avoid stress concentrations and material distortion. There are numerous advantages to using adhesively bonded load-carrying joints. Goland and Reissner's seminal work [1] provided theoretical methods for analysis of adhesive joints. Barenblatt [2] and Dugdale [3] simultaneously proposed the cohesive zone model to study fracture in elastic and elastic–plastic materials. Since then the cohesive zone models have been incorporated into the finite element methods to study the fracture of elastic–plastic and brittle materials (namely, by Needleman [4], Tvergaard and Hutchinson [5], and Xu and Needleman [6]) under static conditions. The concept of the interface element has been used to study the fatigue and durability of the bonded joints for aluminum and steel in the automotive industry [7–9]. Other approaches have been used to study crack growth, and an analytical method was proposed but was limited to the study of test specimens [10]. An experimental and numerical study of laminated angle-ply composites under multidirectional loading was presented [11] and relationships between the slope of the fracture line and the crack growth path were established using finite element for stress analysis.

The cohesive zone model (CZM) has been used in a wide variety of problems involving fracture of adhesively bonded joints. More recently, the interface element approach has been used to study the viscoelastic fracture of polymers by Rahul-Kumar et al. [12]. CZM has also been effectively used to study stable and unstable crack growth under quasi-static loading conditions [13]. The cohesive zone model is essentially a discrete concept, but it can be transformed into a continuum or smeared formulation by distributing the work of separation or fracture energy G_c over the width of an element [14,15]. Smeared representations of the cohesive zone model have been used to study the crack growth and response of mostly homogeneous material [16].

Implementation of the cohesive zone model in a explicit code is something that has not been addressed very well in the open literature. Explicit methods have a marked advantage over implicit methods, especially when it comes to analyzing structures under dynamic loading. The fact that explicit methods do not require iterations to solve a nonlinear problem also makes the analysis much faster in terms of time required for convergence. Adhesives have been used to bond joints in cars for quite some time now. Most of the automobile industry uses LS-DYNA to simulate the car crash and testing of composite material. Keeping this in mind, we undertake the task of incorporating the CZM law in LS-DYNA to help facilitate the study of these bonded joints in a car crash. LS-DYNA does not allow the user to define elements, and so interface elements cannot be incorporated into LS-DYNA. One other way to incorporate the CZM law is through a user-defined material (UMAT) option, which LS-DYNA allows.

A combined computational and experimental study of the response and degradation of an adhesively bonded double-cantilever

Presented as Paper 1961 at the 47th AIAA/ASME/ASCE/AHS/ASC Structures, Structural Dynamics, and Materials Conference, Newport, RI, 1–4 May 2006; received 22 June 2006; revision received 26 April 2007; accepted for publication 1 July 2007.

*Research Assistant, Department of Aerospace and Ocean Engineering; currently Manager, Tata Advanced Materials, Ltd., Bangalore 562 106, India.
†Professor, Department of Aerospace and Ocean Engineering. Associate Fellow AIAA.
‡Professor Emeritus, Department of Aerospace and Ocean Engineering. Senior Member AIAA.
§Adhesive and Sealant Science Professor, Department of Engineering Science and Mechanics.

beam (DCB) subjected to dynamic loading is presented. Both aluminum and composite beams are studied. The adhesive is a two-part elevated cure epoxy. Smeared formulation of the cohesive zone model implemented through a material model in the explicit code LS-DYNA is used to represent the adhesive layer in the DCB. Investigation of adhesive bonds used in structures was investigated experimentally in the early sixties for their strain rate effects and an experimental approach was proposed [17]. In the drop-tower test it is assumed that the velocity imparted to the arms of the DCB adherends is constant [18]. However, in this study it will be shown that for composite DCBs with thin adherends, this assumption does not capture the right crack growth behavior. Incorporation of the displacement history, obtained from digital images of the experiments, in the simulations captures the stick-slip behavior exhibited by the composite DCB.

II. Dynamic Fracture Tests

The materials selected for the adherends of the DCB were 6061 aluminum and a composite. The composite material is an orthotropic plain-weave balanced fabric manufactured by Advanced Composites Group (MTM49/CF0501). Pacific Composites, Inc. fabricated this material into composite panels of the desired layup with a 42% resin content. The adhesive used is a two-part elevated-cure epoxy system produced by Sovereign Speciality Adhesives, Inc. (PL731SI).

The aluminum adherends of the DCB measured $25.4 \times 6.4 \times 254$ mm, were P2-etched to provide an adequate bonding surface, and the bond-line thickness was either 0.8 or 0.5 mm. The surfaces of the composite panels were abraded and cleaned with acetone before bonding, and the bond line was again either 0.8 or 0.5 mm. Both aluminum and composite specimens were cured using the same heating process. The cured composite panels were cut into 254×25.4 mm strips. A hardened steel wedge was used to drive precracks in the adhesive 50–55 mm long. After precracking, holes were drilled and tapped for the end blocks.

The DCB specimens were mounted vertically in a drop tower. Two polycarbonate wedges were attached to the weighted drop-tower sled, with the sled riding on linear bearings to reduce frictional effects. The sled was dropped from a height of approximately 0.7 m, reaching a velocity of 3.7 m/s before striking the specimen. At impact, the wedges contacted bearings of the end blocks attached to the free end of the adherends of the DCB, as depicted in Fig. 1. A photograph of the drop-tower setup is shown in Fig. 2. A high-speed video camera was used to record images of the specimen at 2000 frames per second. No load or displacement measurements were physically made on the specimen. It is known that dynamic load cell measurements are meaningless because of resonances and noise caused by wave propagation and vibration of the adherends. The displacement profile and opening displacement are deduced from the image data at each recorded instant in time. National Instruments LabVIEW software was used to gather opening displacement data from these images. An edge-detection program was used to scan the images to find the x and y coordinates along each beam, as shown in Fig. 3. This program collects data every 10 pixels, or about 4 mm, along an image and calculates the opening displacement δ as the difference between the y coordinates of the upper and lower adherends (y_1 and y_2) subtracted by the half thickness of the beam at numerous points along the specimen. The detection data for all images were imported into an analysis program that scales the displacements from pixels to meters. A nonlinear fit was then applied to the data from each image at each instant in time in the form of

$$\delta = \frac{2P}{3E_f I}[-(a-x)^3 + 3a(a-x)^2] \text{ unit step } [x-a] \qquad (1)$$

where δ is the opening displacement at a given x, P is the calculated load , E_f is the modulus of elasticity of the adherend material, I is the moment of inertia of the adherends, a is the crack length, and x is the position along the beam. The crack length is then extracted and used to calculate the energy release rate by the equation [18]

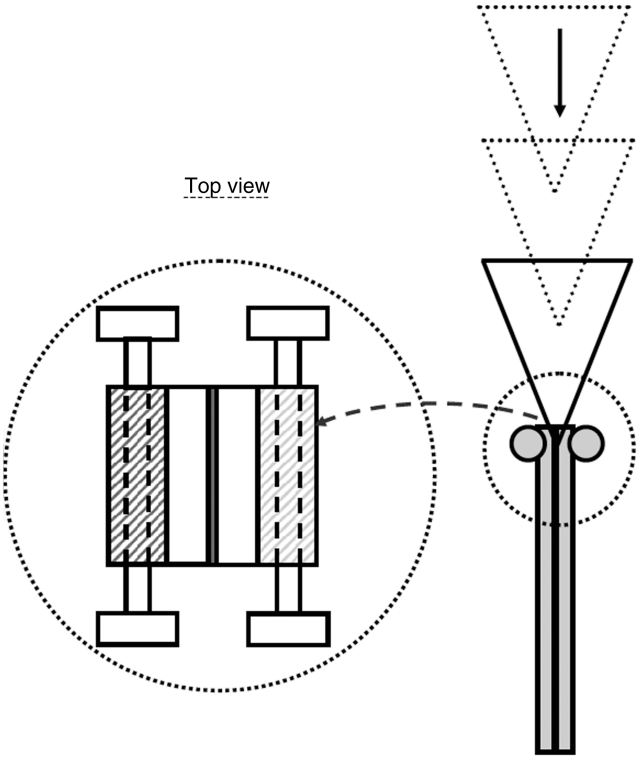

Fig. 1 End block with a bearing and a schematic of the drop tower.

Fig. 2 The drop-tower setup in the Adhesion Science Laboratory.

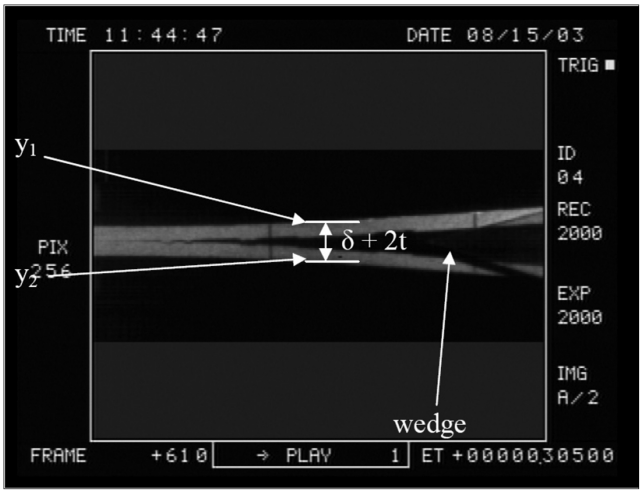

Fig. 3 Parameters collected with the edge-detection program.

$$G_I = \frac{9\Delta^2 E_f I}{4Ba^4} F \tag{2}$$

where Δ is the opening displacement at the load application point, B is the specimen width, and F is a correction factor for large deflection. See [19] for more details on the testing procedure and specimen preparation.

III. Cohesive Zone Model

The CZM was developed by Goyal et al. [20]. This CZM law was developed to model fracture in finite element analysis via user-defined interface elements. Because we implement this law as a UMAT in LS-DYNA, it is necessary to review it here to make this paper self-contained. Let T_3 and Δ_3 denote the mode-I traction and opening displacement, respectively; let T_1 and Δ_1 be the mode-II traction and sliding displacement, respectively; and let T_2 and Δ_2 denote the mode-III traction and out-of-plane sliding displacement, respectively. Under a monotonically increasing mode-I loading only, the traction is related to the opening displacement by

$$T_3 = T_3^c \langle \Delta_3/\Delta_3^c \rangle \exp\left(\frac{1 - \langle \Delta_3/\Delta_3^c \rangle^\beta}{\beta}\right) \tag{3}$$

in which the relative maximum traction T_3^c is attained at the opening displacement Δ_3^c and dimensionless parameter β ($\beta > 0$ is introduced to control the softening behavior of the CZM law). The area under the traction-displacement law (3) equals the critical strain energy release rate in mode I. That is,

$$G_{I_c} = \int_0^\infty T_3 d\Delta_3 = T_3^c \Delta_3^c \psi(\beta) \tag{4}$$

where

$$\psi(\beta) = \beta^{(2-\beta)/\beta} \Gamma\left[\frac{2}{\beta}\right] \exp\left(\frac{1}{\beta}\right) \tag{5}$$

and $\Gamma[z]$ is the Euler gamma function of argument z. For $\beta = 1$, function $\psi = e$ (the base of the natural logarithm) and $G_{I_c} = T_3^c \Delta_3^c e$. For example, specifying the relative maximum traction T_3^c, parameter β, and the critical strain energy release rate, the critical opening displacement Δ_3^c is computed from Eq. (4). The CZM law (3) is plotted versus the opening displacement for several values of β in Fig. 4, in which, for plotting purposes, it is assumed that $T_3^c = 48$ MPa and Δ_3^c 0.002 mm. In Fig. 4, the critical strain energy release rate decreases from 26.1 J/m^2 at $\beta = 1$ to 10.9 J/m^2 at $\beta = 4$. As at $\beta \to \infty$, $\psi \to 1/2$, which perfectly characterizes brittle material behavior. Hence, β is termed a brittleness parameter.

The mode-I CZM law (3) is extended to include resistance to interpenetration of the crack faces and irreversibility. First define

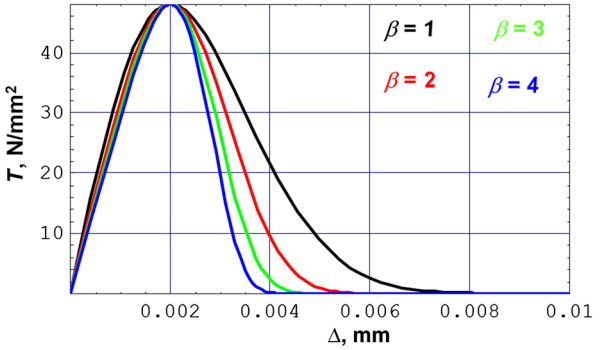

Fig. 4 Effect of β on the mode-I CZM law for a fixed value of the critical opening displacement with $T_c = 48$ MPa.

normalized traction and opening displacements by $\bar{T}_3 \equiv T_3/T_3^c$ and $\bar{\Delta}_3 \equiv \Delta_3/\Delta_3^c$. Resistance to crack face interpenetration allows $T_3 < 0$ if $\Delta_3 < 0$ and irreversibility is modeled by a semipositive dimensionless damage parameter d, determined in terms of $\bar{\Delta}_3$ if $\bar{\Delta}_3 > 1$. The extended mode-I law is

$$\bar{T}_3 = \langle \bar{\Delta}_3 \rangle \exp\left(\frac{2 - [\langle \bar{\Delta}_3 \rangle^\beta]/d - d}{\beta}\right) - \langle -\bar{\Delta}_3 \rangle \exp\left(\frac{1 + \kappa|\bar{\Delta}_3|^\beta}{\beta}\right) \tag{6}$$

where

$$\langle l \rangle = \begin{cases} |l| & \text{if } l > 0 \\ 0 & \text{if } l \le 0 \end{cases} \tag{7}$$

and parameter κ is an interpenetration factor, with $\kappa \ge 1$ to magnify the repulsive traction. For the discrete time steps used in the simulations, the damage parameter is defined as

$${}^{t+\delta t}d = \max\left(1, {}^t d, {}^{t+\delta t}\bar{\Delta}_3^\beta\right) \tag{8}$$

with initial value ${}^0 d = 1$. The damage parameter increases from unity in the undamaged state to infinity for completely damaged material. Equation (6) is equivalent to Eq. (3) if no damage occurs ($d = 1$) or for monotonically increasing loading [$d = (\bar{\Delta}_3)^\beta$]. Complete unloading from the softening portion of the CZM law occurs exponentially back to the origin.

Consider a pure mode-II loading in which $\Delta_1 \neq 0$, $\Delta_2 = 0$, and $\Delta_3 \le 0$. The CZM law for pure mode II is assumed to be

$$\bar{T}_1 = \bar{\Delta}_1 \exp\left(\frac{2 - |\bar{\Delta}_1^\beta|/d - d}{\beta}\right) \tag{9}$$

where $\bar{T}_1 = T_1/T_1^c$ and $\bar{\Delta}_1 = \Delta_1/\Delta_1^c$, and the damage parameter is defined as

$${}^{t+\delta t}d = \max\left(1, {}^t d, {}^{t+\delta t}\bar{\Delta}_1^\beta\right) \tag{10}$$

with initial value ${}^0 d = 1$. Similar to Eq. (4), the critical strain energy release rate is given by

$$G_{\mathrm{II}_c} = \int_0^\infty T_1 d\Delta_1 = T_1^c \Delta_1^c \psi(\beta) \tag{11}$$

with the function $\psi(\beta)$ as given by Eq. (5). For pure mode-III loading in which $\Delta_1 = 0$, $\Delta_2 \neq 0$, and $\Delta_3 \le 0$, the CZM law is the same form as Eqs. (9) and (10), but with subscript $1 \to 2$, and

$$G_{\mathrm{III}_c} = \int_0^\infty T_2 d\Delta_2 = T_2^c \Delta_2^c \psi(\beta) \tag{12}$$

Specifying the adhesive strengths T_1^c, T_2^c, and T_3^c; critical strain energy release rates G_{I_c}, G_{II_c}, and G_{III_c}; and the brittleness parameter β, the critical displacements Δ_3^c, Δ_1^c, and Δ_2^c are determined from Eqs. (4), (11), and (12), respectively.

Finally, consider the CZM law extended to mixed-mode loading conditions $\Delta_i \neq 0$ $(i = 1, 2, 3)$. The magnitude of the resultant normalized traction $\bar{T}_v$ is assumed to be coincident with the normalized displacement vector having components $\bar{\Delta}_i$. Following the pattern of Eqs. (3) and (9), the resultant traction is assumed to be related to the magnitude of the normalized total displacement λ by

$$\bar{T}_v = \lambda \Theta(\bar{\Delta}_i) \tag{13}$$

where

$$\lambda = \sqrt{\bar{\Delta}_1^2 + \bar{\Delta}_2^2 + \bar{\Delta}_3^2} \tag{14}$$

and

$$\frac{\partial \Theta}{\partial \bar{\Delta}_i} < 0 \qquad i = 1, 2, 3 \tag{15}$$

The components of the normalized resultant traction are given by $\bar{T}_j = \bar{T}_v(\bar{\Delta}_j/\lambda)$. Substituting for $\bar{T}_v$ from Eq. (13), we find

$$\bar{T}_j = \bar{\Delta}_j \Theta(\bar{\Delta}_k) \qquad j, k = 1, 2, 3 \tag{16}$$

The decreasing function of the normalized displacements is taken as

$$\Theta(\bar{\Delta}_k) = \exp\left[\frac{2 - \mu^\beta/d - d}{\beta}\right] \tag{17}$$

in which the mixed-mode normalized displacement is defined as

$$\mu = (|\bar{\Delta}_1|^\alpha + |\bar{\Delta}_2|^\alpha + \langle \bar{\Delta}_3 \rangle^\alpha)^{1/\alpha} \qquad \alpha \geq 2 \tag{18}$$

and the damage parameter d is defined by

$$^{t+\delta t}d = \max(1, {}^t d, {}^{t+\delta t}\mu^\beta) \qquad {}^0 d = 1 \tag{19}$$

It is shown [20] that this mixed-mode CZM given by Eqs. (16–19) satisfies the maximum strength criterion

$$\left[\left(\frac{T_1}{T_1^c}\right)^\alpha + \left(\frac{T_2}{T_2^c}\right)^\alpha + \left(\frac{\langle T_3 \rangle}{T_3^c}\right)^\alpha\right]^{\frac{1}{\alpha}} = 1 \tag{20}$$

and that the mixed-mode fracture criterion

$$\left(\frac{G_I}{G_{I_c}}\right)^{\alpha/2} + \left(\frac{G_{II}}{G_{II_c}}\right)^{\alpha/2} + \left(\frac{G_{III}}{G_{III_c}}\right)^{\alpha/2} = 1 \tag{21}$$

The exponent α defines the shape of the failure surface for the onset of failure and the progression of fracture. For exponent $\alpha = 2$, the strength criterion (20) is a quadratic surface in the space of the traction components, and the fracture criterion (21) is a plane in the space of the energy release rate components. Including the interpenetration term, the final form of the CZM law is

$$\begin{bmatrix} \bar{T}_1 \\ \bar{T}_2 \\ \bar{T}_3 \end{bmatrix} = \begin{bmatrix} \bar{\Delta}_1 \\ \bar{\Delta}_2 \\ \bar{\Delta}_3 \end{bmatrix} \Theta(\bar{\Delta}_k) - \begin{bmatrix} 0 \\ 0 \\ -\langle -\bar{\Delta}_3 \rangle \end{bmatrix} \exp\left(\frac{1 + \kappa|\bar{\Delta}_3|^\beta}{\beta}\right) \tag{22}$$

The mixed-mode CZM law (22) reduces to the single-mode CZM laws given by Eqs. (6) and (9) (in which, in the latter equation, subscripts 1 and 2 are interchangeable).

IV. Implementation of CZM Through Material Definition

LS-DYNA does not have the option for the user to define new elements, so implementing the CZM law in an interface element, as was done in [20], is not feasible. The only way to incorporate the CZM law is through the UMAT option in LS-DYNA. Hence, the CZM law is incorporated through the material definition in standard library elements. The plane strain or solid brick elements in the library are used to model the adhesive with the thickness of the adhesive elements, denoted by h, equal to either 0.8 or 0.5 mm in the test specimens. For the example of a single plane strain adhesive element, shown in Fig. 5, the mode-I opening displacement $\Delta_3 = \Delta h$ and the in-plane sliding displacement $\Delta_1 = h\Delta\phi$. The interpenetration term in Eq. (22) is activated if $\Delta h < 0$. A brick element referenced to Cartesian coordinates x, y, and z is depicted in Fig. 6, with mode I determined by extension along the y axis, mode II determined by the shear strain in the x–y plane, and mode III determined by the shear strain in the x–z plane.

The UMAT subroutine outputs the stress vector to the main program of LS-DYNA. Based on the orientation of the fracture modes shown in Fig. 6 and the equations for the traction-displacement law from Eq. (22), the stress vector can be defined as

$$\begin{bmatrix} \sigma_{xx} \\ \sigma_{yy} \\ \sigma_{zz} \\ \tau_{xy} \\ \tau_{yz} \\ \tau_{zx} \end{bmatrix} = \begin{bmatrix} 0 \\ T_3^c \langle \bar{\Delta}_3 \rangle \exp\left(\frac{2-\mu^\beta/d-d}{\beta}\right) - T_3^c \langle -\bar{\Delta}_3 \rangle \exp\left(\frac{1+\kappa|\bar{\Delta}_3|^\beta}{\beta}\right) \\ 0 \\ T_2^c \bar{\Delta}_1 \exp\left(\frac{2-\mu^\beta/d-d}{\beta}\right) \\ 0 \\ T_1^c \bar{\Delta}_2 \exp\left(\frac{2-\mu^\beta/d-d}{\beta}\right) \end{bmatrix} \tag{23}$$

The displacements are calculated from the strain vector that comes as information after every time step from the main program. LS-DYNA is programmed based on the Eulerian formulation [21], and so the strains at every step are calculated taking the deformed state of the element at the previous time step as the reference state. This has to be taken into account when evaluating the opening displacements in the UMAT subroutine. Because it is assumed that the stress components σ_{xx}, σ_{zz}, and τ_{yz} vanish in Eq. (23), the strains conjugated to these stress components are neglected.

The modeling of the precrack required some special attention in the numerical analysis. The material defined for adhesives was modified a little for the precrack elements. The modified material offered no resistance in all the opening modes (i.e., all the stresses were zero) and only offered resistance for interpenetration ($\bar{\Delta}_3 < 0$).

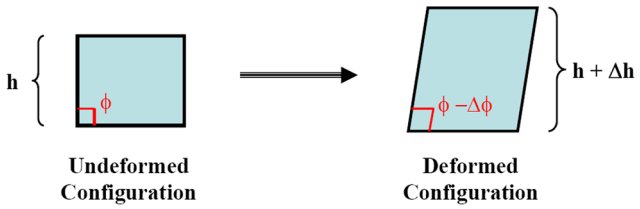

Fig. 5 Calculation of the opening displacements in a plane strain element.

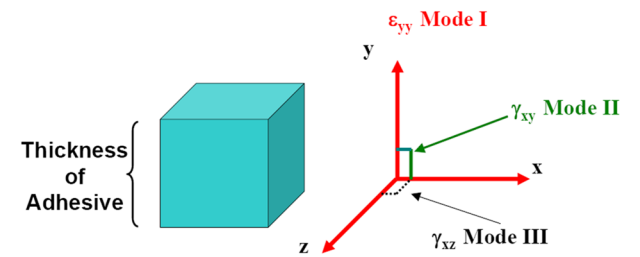

Fig. 6 Reference orientation for the three fracture modes in a standard brick element.

V. Results and Discussion

A. Aluminum DCB

The material properties for the aluminum are $E = 69$ GPa, $\nu = 0.3$, and $\rho = 2700$ kg/m^3.

The adhesive properties used in this simulation are the same as those used for the quasi-static testing, as follows: $T_3^c = 40$ MPa, $T_1^c = T_2^c = 60$ MPa, $G_{I_c} = 2.2$ N/mm, $G_{II_c} = G_{III_c} = 2.8$ N/mm, α=2, β=2, $\kappa = 10^6$ N/mm^3, and $\rho = 1000$ kg/m^3. An average opening velocity of 2.2 m/s was induced at the tips of the beams, due to the falling wedge. The calculations for these were made based on the angle of the wedge, the falling mass on top of the drop tower. The main assumption here is that the wedge is in constant contact with the bearings. Details of these calculations can be found in [22].

A two-dimensional plane strain model was used for numerical analysis of the aluminum DCB. The adhesive was modeled with plane strain elements too, but the material was user-defined. Single elements through the thickness were used to model the adhesive, with the height of the element being kept equal to the thickness of the adhesive. The length of the element was kept as 0.5 mm. The geometry and loading of the specimen is shown in Fig. 7. The length of the specimen was 254 mm, the width W was 25.4 mm, and the thickness h of the adherends was 6.35 mm.

Figure 8 shows the comparison of the crack lengths for two experiments and a numerical simulation. The graph shows that the crack lengths predicted from the numerical analysis are in good agreement with the experimental results. On careful observation it might be noticed that at some places, the crack lengths deduced from the experiments start to reduce marginally with increasing time. This is physically not possible because the material once cracked cannot heal again. The error is induced from the numerical root finding of Eq. (1) used to get the crack length from the digital image captured.

B. Composite DCB

Having established the CZM law for the adhesive through the UMAT option in LS-DYNA, we proceed to analyze joints for composite adherends. The additional failure modes for a composite DCB are the failure of the composite material and the delamination between the plies. The failure of the composite material is considered in this simulations, but the delamination between the plies is ignored. For the degradation of the composite material, the Tsai and Wu model [23], which takes into account the fiber failure as well as the matrix failure, is considered. The material model for the degradation of the composite material is already incorporated in LS-DYNA through the defined material type 55 (*MAT_054-55).

The geometry of the composite DCB specimen is the same as that of the aluminum DCB, except that the thickness of the adherends is 2.34 mm. Here, the composite material is a woven composite made up of 11-ply symmetric layup. The material properties for the 11-ply composite material are as follows: E_{11}=45 GPa, $E_{22} = E_{33}$=40 GPa, $\nu_{21} = \nu_{31}$=0.24, ν_{32}=0.34, G_{12}=18 GPa, and $G_{13} = G_{23}$=14 GPa.

The same setup for the drop tower was used as for the aluminum DCB. However, when the digital images were processed to deduce the crack information, the trend shown by the crack growth in the composite DCB was altogether different from the crack growth pattern in the aluminum DCB. The crack growth information is shown in Fig. 9

As can be seen from Fig. 9, the crack growth exhibits some kind of stick-slip behavior. The flat plateau observed in the graph indicates that, for a certain period of time, the crack is arrested. Also the reduction in crack growth observed once again contributes to the numerical error in obtaining the crack lengths from the digital images.

The LS-DYNA simulations were carried out a little differently from the aluminum DCB. Plane strain elements cannot be used to model composite beams, and so shell elements were used to model the composite beams and the adhesive was modeled using 3D brick elements. The crack length was measured at the center of the width of the composite DCB. A crack growth pattern similar to that for the aluminum DCB was obtained. This led us to look closely at each of our assumptions that were made at every step of the way in the experiments as well as in the numerical analysis. One of the major assumptions made in the drop-tower experiment was that the wedge stayed in continuous contact with the bearings and the velocity imparted to the bearings by the falling wedge was constant. To verify this assumption, the tip displacement of the adherends were plotted with respect to time from the digital images that were taken of the experiment. The tip displacement is shown in Fig. 10. As can be seen, the tip displacement is not exactly linear, which indicates that the velocity is not constant. However, looking at the graph in Fig. 10, one can argue that it is almost linear. A linear regression fit was done to check this. The fit is plotted along with the original curve in Fig. 10. The parameter R^2, which is known as the measure of the goodness of the fit, is very close to unity (the exact fit). However, the good fit does not necessarily convey that the assumptions made, keeping in mind the physics of the problem, are indeed valid. If the wedge loses contact with the bearings for very small period of times, the effect may not be noticed in the tip displacement, because it may be too fast for the camera to capture, but it could change the way the crack grows.

To be certain about the effects of this nonlinear displacement profile exhibited by the arms of the composite adherends, a simulation in LS-DYNA was done in which instead of prescribing a

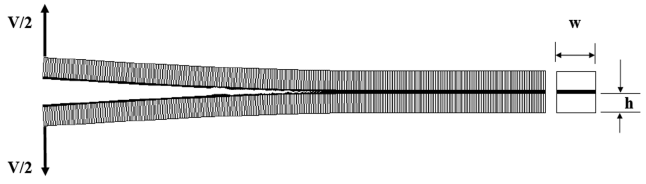

Fig. 7 Geometry of the DCB specimen.

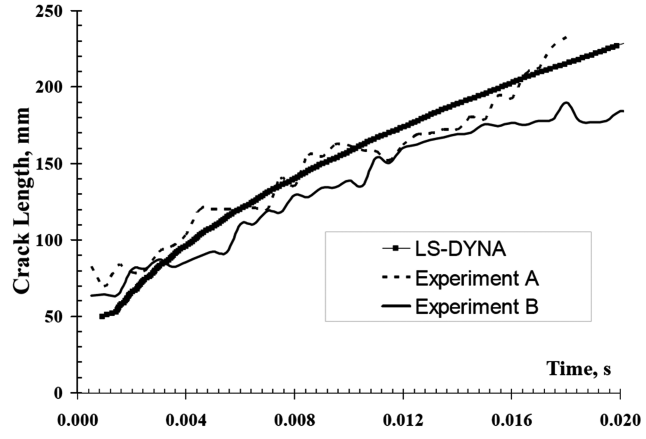

Fig. 8 Crack-length comparison for an aluminum DCB in a drop tower test.

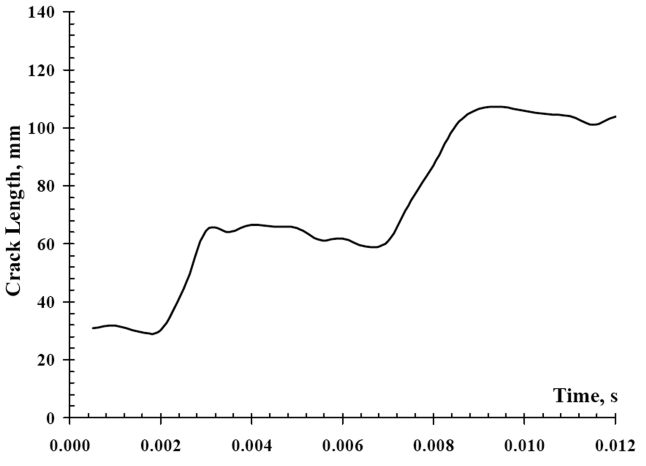

Fig. 9 Crack length for a composite DCB test in the drop tower.

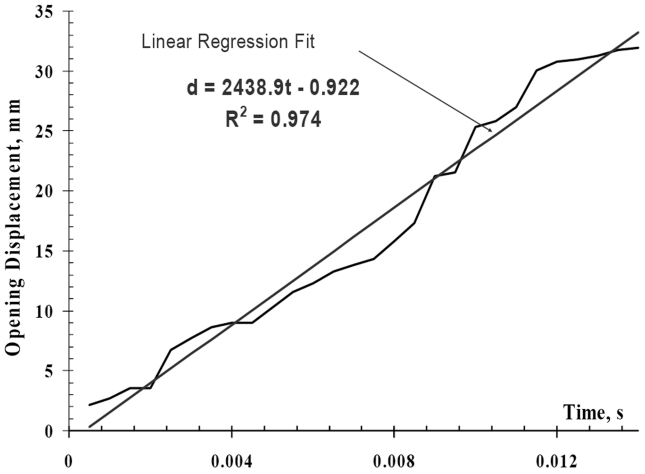

Fig. 10 Tip displacement observed from the test and a linear regression fit.

constant velocity at the tips of the adherends, the displacement profile measured from the camera was prescribed as the boundary condition. Surprisingly, the crack growth pattern that this simulation gave us was different from the one with the constant velocity. It exhibited the stick-slip behavior, as shown in the experiments. This is a very important observation, because any study in the literature that has used the drop tower has assumed that the velocity imparted by the falling wedge to the bearings is constant. Here, it is shown that for the smallest period of time when a bearing loses contact with the wedge, it will change the crack growth pattern. There is a possibility that this will also depend somewhat on the compliance of the adherends: if the adherends are too compliant (i.e., if they are too thin), there is a high possibility of losing contact with the wedge.

The crack growth pattern obtained from the simulation by prescribing the displacement observed in the experiments at the tips is shown in Fig. 11. For the sake of comparison and completeness, the results obtained from numerical simulations using constant tip velocity are also presented. As can be seen, the crack growth using a constant tip velocity is monotonically increasing without any stick-slip behavior. One can observe that the predominant effect in the stick-slip behavior is due to the application of the experimentally measured tip displacement profile.

VI. Conclusions

The results from the CZM law implemented through a material model in an explicit commercial code correlates well with the crack growth observed in experiments for both the aluminum and composite DCB tested under dynamic loading in the drop tower. For the composite DCB tested in the drop tower, the assumption of constant velocity imparted by the falling wedge to the bearings does not predict the right crack growth behavior. The displacement history obtained from the digital images was used as the loading history to capture the stick-slip behavior exhibited by the composites.

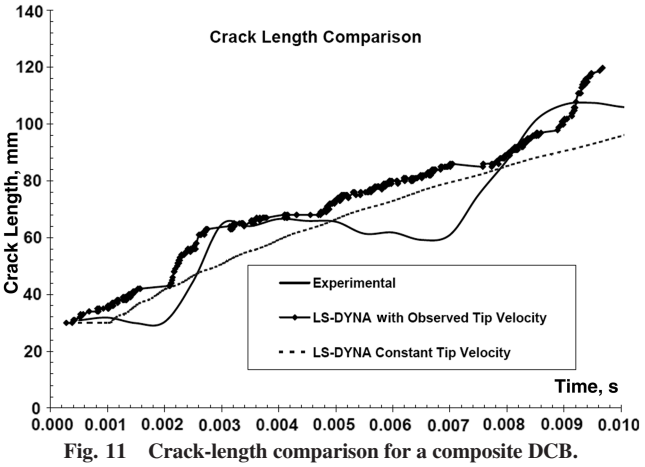

Fig. 11 Crack-length comparison for a composite DCB.

Acknowledgments

This research is supported, in whole or in part, by the Automotive Composite Consortium's U.S. Department of Energy Cooperative Agreement no. DE-FC05-95OR22363. Such support does not constitute an endorsement by the U.S. Department of Energy of the views expressed here. The authors would like to thank Josh Simón from the Engineering Science and Mechanics department at Virginia Polytechnic Institute and State University for providing us with the experimental data. In addition, we would like to thank the project monitor Naveen Rastogi for technical discussions held with him.

References

[1] Goland, M., and Reissner, E., "The Stresses in Cemented Joints," *Journal of Applied Mechanics*, Vol. 11, No. 1, 1944, pp. A17–A27.

[2] Barenblatt, G. I., "The Mathematical Theory of Equilibrium of Cracks in Brittle Fracture," *Advances in Applied Mechanics*, Vol. 7, No. 1, 1962, pp. 55–129.

[3] Dugdale, D. S., "Yielding of Steels Sheets Containing Slits," *Journal of the Mechanics and Physics of Solids*, Vol. 8, No. 2, 1960, pp. 100–104. doi:10.1016/0022-5096(60)90013-2

[4] Needleman, A., "An Analysis of Decohesion Along an Imperfect Interface," *International Journal of Fracture*, Vol. 42, No. 1, 1990, pp. 21–40. doi:10.1007/BF00018611

[5] Tvergaard, V., and Hutchinson, J. W., "The Relation Between Crack Growth Resistance and Fracture Process Parameters in Elastic–Plastic Solids," *Journal of Mechanics and Physics of Solids*, Vol. 40, No. 6, 1992, pp. 1377–1397.

[6] Xu, X.-P., and Needleman, A., "Numerical Simulations of Dynamic Interfacial Crack Growth Allowing for Crack Growth Away From the Bond Line," *International Journal of Fracture*, Vol. 74, No. 4, 1995, pp. 289–324.

[7] Curley, A. J., Jethwa, J. K., Kinloch, A. J., and Taylor, A. C., "The Fatigue And Durability Behaviour Of Automotive Adhesives, Part 3: Predicting the Service Life," *The Journal of Adhesion*, Vol. 66, No. 1, 1998, pp. 39–59.

[8] Dickie, R. A., Haack, L. P., Jethwa, J. K., Kinloch, A. J., and Watts, J. F., "The Fatigue and Durability Behaviour of Automotive Adhesives, Part 2: Failure Mechanisms," *The Journal of Adhesion*, Vol. 66, No. 1, 1998, pp. 1–37.

[9] Jethwa, J. K., and Kinloch, A. J., "The Fatigue and Durability Behaviour of Automotive Adhesives, Part 1: Fracture Mechanics Tests," *The Journal of Adhesion*, Vol. 61, No. 1, 1997, pp. 71–95.

[10] Freiman, S. W., Mulville, D. R., and Mast, P. W., "Crack Propagation Studies in Brittle Materials," *Journal of Materials Science*, Vol. 8, No. 11, 1973, pp. 1527–1533. doi:10.1007/BF00754886

[11] Tirosh, J., Mast, P. W., Beaubien, L., Mulville, D. R., Sutton, S., and andWolock, I., "Fracture Criteria of Fibrous Laminated Composites Under In-Plane Multidirectional Loading," *Journal of Applied Mechanics*, Vol. 47, No. 4, 1980, pp. 563–569.

[12] Rahul-Kumar, P., Jagota, A., Bennison, S. J., and Saigal, S., "Cohesive Element Modeling of Viscoelastic Fracture Application to Peel Testing of Polymers," *International Journal of Solids and Structures*, Vol. 37, No. 13, 2000, pp. 1873–1897. doi:10.1016/S0020-7683(98)00339-4

[13] Makhecha, D. P., Kapania, R. K., Johnson, E. R., Dillard, D. A., and Simón, J., "Modeling Stable and Unstable Crack Growth Observed in Quasi-Static Adhesively Bonded Beam Tests," ASME International Mechanical Engineering Congress and Exposition, Anaheim, CA, American Society of Mechanical Engineering Paper IMECE2004-59765, Nov. 13–19 2004.

[14] Pietruszczak, S., and Mróz, M., "Finite Element Analysis of Deformation of Strain Softening Materials," *International Journal for Numerical Methods in Engineering*, Vol. 17, No. 3, 1981, pp. 327–334. doi:10.1002/nme.1620170303

[15] Bažant, Z. P., and Oh, B., "Crack Band Theory for Fracture of Concrete," *Materials and Structures*, Vol. 16, No. 3, 1983, pp. 155–177.

[16] de Borst, R., "Numerical Aspects of Cohesive Zone Models," *Engineering Fracture Mechanics*, Vol. 70, No. 14, 2003, pp. 1743–1757.
doi:10.1016/S0013-7944(03)00122-X

[17] Ripling, J. E., Mostovoy, S., and Patrick, R. L., "Measuring Fracture Toughness of Adhesive Joints," *Materials Research and Standards*, Vol. 4, No. 3, 1964, pp. 129–134.

[18] Blackman, B. R. K., Dear, J. P., Kinloch, A. J., MacGillivray, H., Wang, Y., Williams, J. G., and Yayla, P., "The Failure of Fibre Composites and Adhesively Bonded Fibre Composites Under High Rates of Test, Part 1: Mode I Loading–Experimental Studies," *Journal of Material Science and Technology (Sofia)*, Vol. 30, No. 23, 1995, pp. 5885–5900.

[19] Simon, J. C., Johnson, E. R., and Dillard, D. A., "Characterizing Dynamic Fracture Behavior of Adhesive Joints Under Quasi-Static and Impact Loading," *Journal of ASTM International*, Vol. 2, No. 7, 2005, pp. 34–53
doi:10.1520/JAI12955.

[20] Goyal, V. K., Johnson, E. R., and Davila, C. G., "Irreversible Constitutive Law for Modeling the Delamination Process Using Interfacial Surface Discontinuities," *Composite Structures*, Vol. 65, No. 3, 2004, pp. 289–305.

[21] Anon., *LS-DYNA Theory Manual Version 970*, Livermore Software Technology Corp., Livermore, CA, 2003.

[22] Simón, J. C., "Response and Failure of Adhesively Bonded Automotive Composite Structures Under Impact Loads," M.S. Thesis, Virginia Polytechnic Inst. and State Univ., Blacksburg, VA, 2004.

[23] Tsai, S. W., and Wu, E. M., "A General Theory of Strength for Anisotropic Materials," *Journal of Composite Materials*, Vol. 5, No. 1, 1971, pp. 58–80.
doi:10.1177/002199837100500106

B. Balachandran
Associate Editor